Received: 1 February 2024 | Revised: 9 April 2024 | Accepted: 25 June 2024

DOI: 10.1002/mop.34259

RESEARCH ARTICLE

WILEY

Compact IPD bandpass filter with wide upper stopband based on modified topology for 5G applications

Qi Zhang | **Yazi Cao** | **Gaofeng Wang**

MOE Engineering Research Center of Smart Microsensors and Microsystems, School of Electronics and Information, Hangzhou Dianzi University, Hangzhou, China

Correspondence
Yazi Cao, School of Electronics and Information, Hangzhou Dianzi University, Hangzhou, China.
Email: caoyazi@hdu.edu.cn

Funding information
National Natural Science Foundation of China, Grant/Award Numbers: 92373202, 62141409; National Key Research and Development Program of China, Grant/Award Number: 2019YFB2205003; Zhejiang Provincial Key Research & Development Project, Grant/Award Number: 2021C01041

Abstract

A compact bandpass filter (BPF) with wide stopband performance is proposed and implemented on Si-based integrated passive device (IPD) technology. A modified topology consisting of a novel Pi-section and two capacitors are introduced in this BPF. The Pi-section topology can achieve a band-pass performance and generate four transmission zeros out-of-band. These two capacitors can improve the in-band matching and also widen the stopband. The proposed BPF with a compact size of 1.0 mm × 0.5 mm × 0.3 mm is fabricated using Si IPD technology and measured by on-wafer probing. It shows that the insertion loss is less than 1.75 dB, the return loss is better than 18 dB in the 5G band, and the upper stopband suppression level is better than 17.5 dB up to 18 GHz. The simulated and measured results of the proposed BPF are in reasonably good agreement.

KEYWORDS

bandpass filter (BPF), high out-of-band rejection, Pi-section, transmission zero

1 | INTRODUCTION

Bandpass filters (BPFs) with compact size, high frequency selectivity, low cost, wide stopband and higher integration are vital in modern wireless communication.[1–3] BPFs based on different technologies have been reported, such as stepped-impedance stubs,[4] coupling structure,[5] and electromagnetic bandgap[6] on LTCC technology, coupled line Resonator on CMOS technology,[7] and Pi-section,[1] stepped-impedance multimode resonator[8] and electric and magnetic coupling resonators[9] on IPD technology.

In LTCC technology,[4–11] the large chip size and complex fabrication process affect the massive production yield of the BPF. These filters based on the coupled line resonators also have large chip size and therefore they are only suitable for millimeter wave band.[7,9] IPD technology[1,8,10] has advantages over LTCC technology in the chip size and high out-of-band rejection performance. The BPF with high rejection and small size is still a hot topic. Many studies in different technologies have been reported to widen the BPF stopband, including lump method,[1] coupled line,[2] and multimode resonators.[8] However, all these BPFs require a large electrical size to improve the out-of-band rejection.

In this work, a compact 5G BPF with wide upper stopband is fabricated using Si IPD technology to overcome the issues mentioned above. A modified topology based on a novel Pi-section is introduced to generate three transmission zeros in the out-of-band. A main capacitor and a grounded capacitor are added to this topology to improve the in-band matching and widen the stopband. The proposed BPF is of compact size of 1.0 mm × 0.5 mm × 0.3 mm, and its upper stopband suppression level is better than 17.5 dB up to 18 GHz.

2 | DESIGN AND ANALYSIS

The proposed BPF topology with wide upper stopband is shown in Figure 1. It consists of a novel Pi-section and two capacitors, C_9 and C_{10}. The proposed novel Pi-section topology consists of three transmission-zero resonators. The modified transmission-zero resonator with C_5 in the main branch is shown in Figure 2A. From Figure 2B, this resonator with C_5 in the main branch can achieve a band-pass performance with two transmission zeros. The traditional one without C_5 can only generate a transmission zero at the upper band. Another modified transmission-zero resonator with grounded C_2 in the shunt branch is shown in Figure 2C. From Figure 2D, the traditional one without C_2 can only generate one transmission zero in DC, while the modified resonator with grounded C_2 can generate a transmission zero in the lower band.

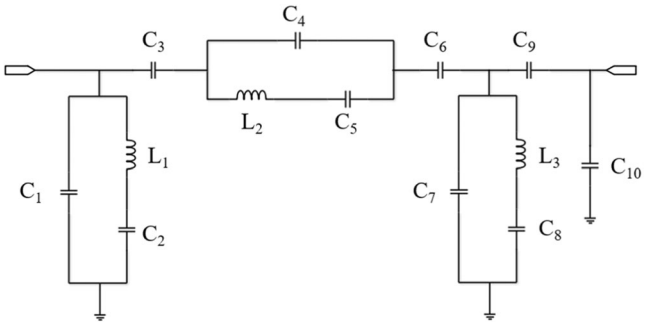

FIGURE 1 Proposed bandpass filter topology.

To analyze how the transmission zeros are generated by the modified transmission-zero resonator, the ABCD matrix of its two ports network can be implemented here. For the modified transmission-zero resonator in the main branch, one has

$$\begin{pmatrix} A & B \\ C & D \end{pmatrix} = \begin{pmatrix} 1 & Z \\ 0 & 1 \end{pmatrix} = \begin{pmatrix} 1 & \frac{1-\omega^2 L_2 C_5}{j\omega(C_4+C_5-\omega^2 L_2 C_4 C_5)} \\ 0 & 1 \end{pmatrix}, \quad (1)$$

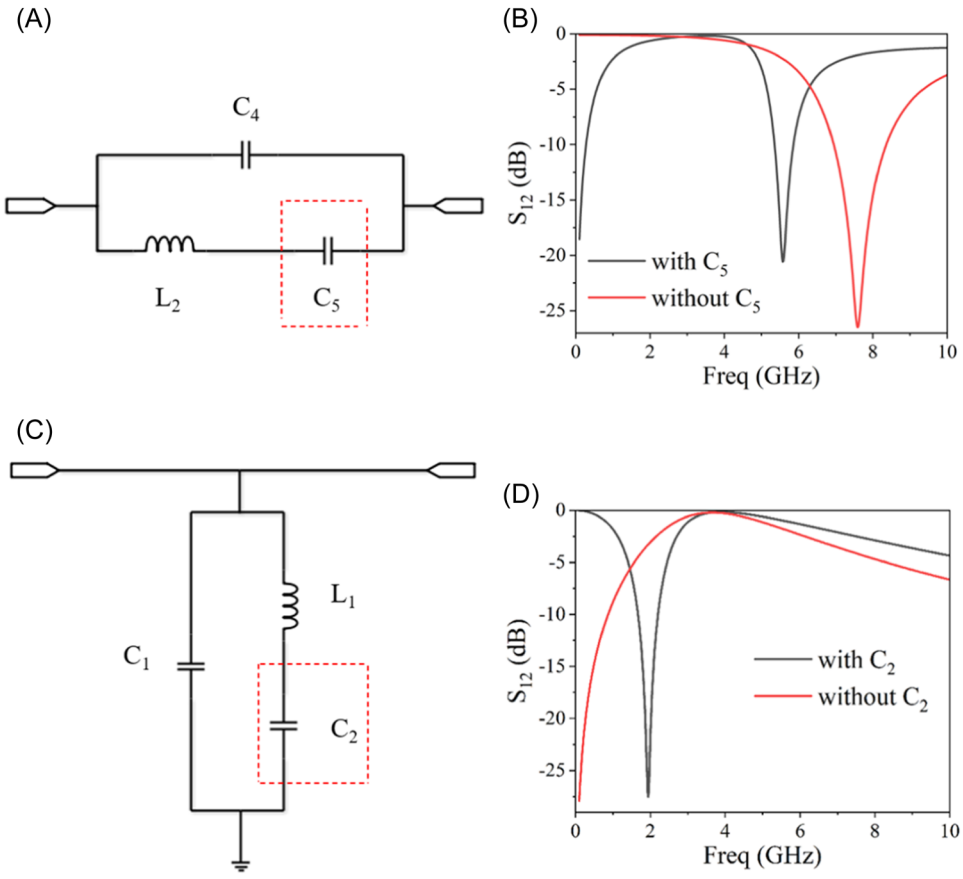

FIGURE 2 Simulated results of traditional versus modified transmission-zero resonators. (A) Traditional (without C_5) versus modified (with C_5) resonators in the main branch. (B) Simulated results of the traditional (without C_5) versus modified (with C_5) resonators in the main branch. (C) Traditional (without C_2) versus modified (with C_2) ground resonators. (D) Simulation results of traditional (without C_2) versus modified (with C_2) ground resonators.

where ω is the transmission frequency of the filter. The S parameter S_{12} related to the ABCD matrix is given as follow:

$$S_{12} = \frac{2(AD - BC)}{A + B/Z_0 + CZ_0 + D}. \quad (2)$$

When $S_{12} = 0$, the values of ω can be determined as

$$\begin{cases} \omega_1 = 0 \\ \omega_2 = \sqrt{\frac{C_4 + C_5}{L_2 C_4 C_5}}, \end{cases} \quad (3)$$

where $C_4 = 0.57$ pF, $C_5 = 0.63$ pF, and $L_2 = 2.7$ nH in the proposed modified resonator. The two transmission zeros are in DC and 5.59 GHz, respectively.

For the modified transmission-zero resonator in the shunt branch, one has

$$\begin{pmatrix} A & B \\ C & D \end{pmatrix} = \begin{pmatrix} 1 & 0 \\ Y & 1 \end{pmatrix} = \begin{pmatrix} 1 & 0 \\ \frac{j\omega(C_1 + C_2 - \omega^2 L_1 C_1 C_2}{1 - \omega^2 L_1 C_2} & 1 \end{pmatrix}. \quad (4)$$

According to Equation (1), the value of ω can be determined as

$$\omega = \sqrt{L_1 C_2}, \quad (5)$$

where $C_1 = 1.93$ pF, $C_2 = 3.53$ pF, and $L_1 = 1.9$ nH. The transmission zero is at 1.95 GHz.

The performance of the novel Pi-section topology, which consists of three transmission-zero resonators, is herein analyzed. Three modified transmission-zero resonators are introduced in the Pi-section topology, as shown in Figure 3A. It includes two modified transmission-zero resonators in the shut branches and one modified resonator in the main branch. As shown in Figure 3B, two transmission zeros are generated in the lower band, and one transmission zero is located in the upper band. Moreover, two poles can be generated in the passband. And it is possible to move one of the transmissions zero to a lower frequency point to further increase the suppression level. However, to obtain a better roll-off coefficient, these two transmission zeros of the low frequency are designed closer to the passband.

Based on the analysis above, the ABCD matrix can be given as follows:

$$\begin{aligned} \begin{pmatrix} A & B \\ C & D \end{pmatrix} &= \begin{pmatrix} 1 & 0 \\ Y_1 & 1 \end{pmatrix} \begin{pmatrix} 1 & \frac{1}{j\omega C_3} \\ 0 & 1 \end{pmatrix} \begin{pmatrix} 1 & Z_1 \\ 0 & 1 \end{pmatrix} \begin{pmatrix} 1 & \frac{1}{j\omega C_6} \\ 0 & 1 \end{pmatrix} \begin{pmatrix} 1 & 0 \\ Y_2 & 1 \end{pmatrix} \\ &= \begin{pmatrix} 1 + \frac{Y_2}{j\omega C_6} + Y_2 Z_1 + \frac{Y_2}{j\omega C_3} & \frac{1}{j\omega C_6} + Z_1 + \frac{1}{j\omega C_3} \\ Y_1 + \frac{Y_1 Y_2}{j\omega C_6} + Y_1 Y_2 Z_1 + \frac{Y_1 Y_2}{j\omega C_3} + Y_2 & \frac{Y_1}{j\omega C_6} + Y_1 Z_1 + \frac{Y_1}{j\omega C_3} + 1 \end{pmatrix}, \end{aligned} \quad (6)$$

where

$$Y_1 = \frac{j\omega(C_1 + C_2 - \omega^2 L_1 C_1 C_2)}{1 - \omega^2 L_1 C_2}.$$

$$Z_1 = \frac{1 - \omega^2 L_2 C_5}{j\omega(C_4 + C_5 - \omega^2 L_2 C_4 C_5)}.$$

$$Y_2 = \frac{j\omega(C_7 + C_8 - \omega^2 L_3 C_7 C_8)}{1 - \omega^2 L_3 C_8}.$$

When $S_{12} = 0$, the transmission zeros can be obtained. Three transmission zeros are located at 1.88, 2.31, and 5.35 GHz, respectively.

As shown in Figure 4, the proposed BPF can achieve three transmission zeros. Two of them are located in the lower band and the third one is located in the upper band. From the simulation, it shows that the impedance match in the passband can be improved and there are three poles when C_9 is added. The two modified transmission-zero resonators in the shut branches can generate two transmission zeros and two transmission

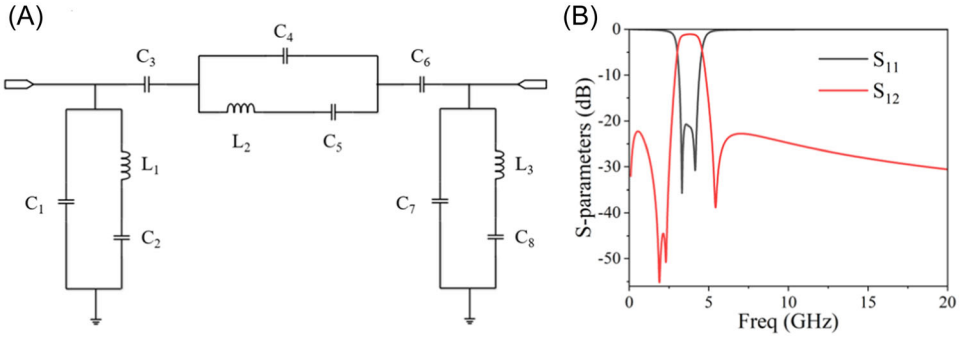

FIGURE 3 Simulated results of the modified novel Pi-type bandpass filter. (A) Topology and (B) simulated S-parameters.

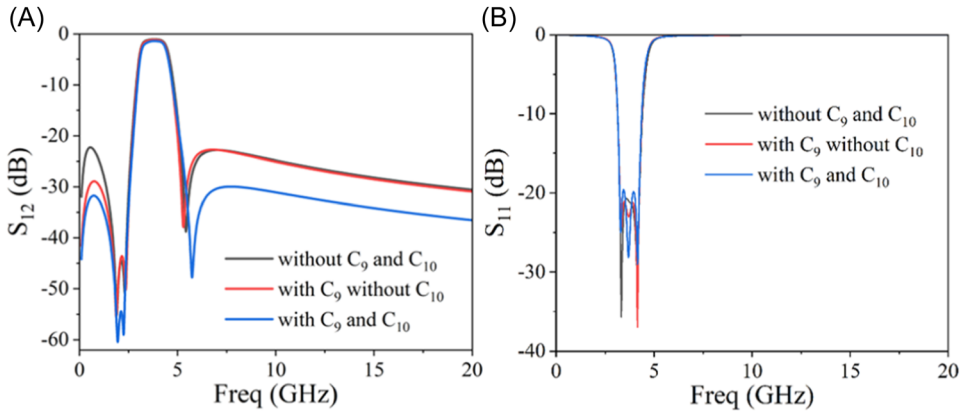

FIGURE 4 Simulation results of the proposed BPF with or without C_9 and C_{10}. (A) Simulated S_{12} and (B) simulated S_{11}.

poles. Besides, the modified transmission-zero resonators in the main road can generate one transmission zero and can generate one transmission pole by cascade C_9. Moreover, when the grounded C_{10} is added, the out-of-band rejection can be greatly improved in the upper band and the out-of-band suppression performance can be also improved in the lower band at the same time. Without C_9 and C_{10}, the locations of the transmission zeros are impacted, and the out-of-band suppression performance becomes worse by comparison to the proposed topology with C_9 and C_{10}. Therefore, the proposed Pi-section topology can achieve the bandpass performance, in which C_9 can improve impedance match in the passband and the out-of-band suppression performance can be improved by adding the grounded C_{10}.

3 | FABRICATION AND EXPERIMENTAL RESULTS

The proposed BPF is fabricated in Si-based IPD technology. Figure 5A shows the cross-section view of the used Si-based IPD technology. The Si substrate layer has a thickness of 250 μm, a relative dielectric constant εr of 11.69, and a loss tangent tanδ of 0.003. The oxide layer is of a thickness of 0.1 μm, a relative dielectric constant εr of 3.9, and a loss tangent tanδ of 0.01. The Si-based IPD technology includes three Cu metal layers, that is, M1, M2, and M3 with thicknesses of 2, 6, and 8 μm, respectively. The inductors are fabricated on the M3 layer. The MIM capacitors are fabricated on the M1 and M2 layers, which are separated by a dielectric layer of a relative dielectric constant εr of 7.46 and a loss tangent tanδ of 0.002.

The proposed BPF is simulated and its GDS layout is generated by the full-wave electromagnetic simulator, UltraEM, from Faraday Dynamics.[12] The micrograph of the fabricated Si-based BPF is shown in Figure 5B. The layout size of the fabricated BPF chip is 1.0 mm × 0.5 mm (0.043 λg × 0.0215 λg). Compared to the circuit level simulation, the electromagnetic level simulation can achieve four transmission zeros generated in the out-of-band. This extra transmission zero is generated outside the high band due to the influence of the parasitic parameters in the layout. The simulated and measurement results of the proposed BPF are compared in Figure 5C. A good agreement between the simulated and measured results is observed.

The fabricated BPF is measured on-chip using the Keysight N5244A PNA-X vector network analyzer and Cascade summit-11000 probe station. And we applied the SOLT de-embedding method during the measurement process, which is based on a 12-item error model and can reduce the impact of system errors on the measurement results. From the measured results, the insertion loss is less than 1.75 dB, the return loss is better than 18 dB in the 5G Sub-6G band, and the upper stopband suppression level is better than 17.5 dB up to 18 GHz (4.8 f_0). As shown in Figure 5, the first parasitic passband in the upper transition band is at around 19.5 GHz.

Table 1 summarizes the performance of the designed BPF. It is observed that the proposed BPF can achieve a compact size (relative to the maximum wavelength) in comparison with other designs. The proposed BPF has lower insertion loss compared with those from references 1 and 4. The proposed BPF can achieve a wider stopband compared with those from references 4, 5, 7 and 10. It is worth mentioning that the quoted on-chip BPF designs are more used in the mm-wave band and 77 band, while this proposed design has more advantages in the 5G sub-6G band.

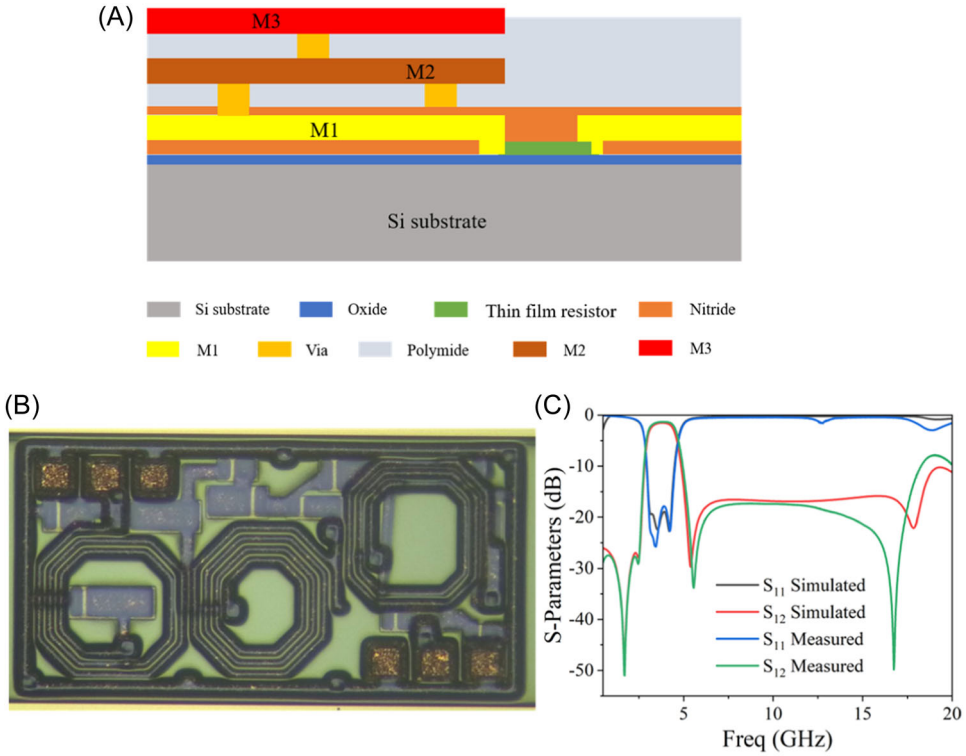

FIGURE 5 (A) Si IPD layer stack-up, (B) micrograph of the proposed BPF, and (C) EM simulated and measured results of the proposed BPF.

TABLE 1 Performance of the proposed BPF versus other BPFs.

Ref.	f_0 (GHz)	Insertion loss (dB)	Size (mm^2)	TZs	Upper stopband (dB)	Process
1	3	1.77	1.63 × 0.62	3	$20/34.6f_0$	GaAs IPD
4	3.5	1.35	6.1 × 6.8	5	$20/2.2f_0$	LTCC
5	0.976	1.96	5.7 × 3.4	3	$30/2.46f_0$	LTCC
7	30	1.66	0.11 × 0.086	2	$25.4/2.3f_0$	CMOS
10	1.56	0.38	0.800 × 0.988	2	$17.4/3.2f_0$	GaAs IPD
This work	3.75	1.75	1.0 × 0.5	4	$18/4.8f_0$	Si-based IPD

Abbreviations: BPF, bandpass filter; IPD, integrated passive device.

4 | CONCLUSION

A compact BPF with high out-of-band rejection has been designed and fabricated on the Si-based IPD technology. By introducing a modified resonator, a BPF topology based on a novel Pi-section has been proposed. The working principles of this modified resonator and the proposed BPF have been further investigated. A grounded capacitor has been introduced in the proposed BPF to achieve wide stopband performance. The proposed BPF has been measured by on-wafer probing with GSG probes. The simulated and measured results of the proposed BPF are in reasonably good agreement. This proposed BPF with high out-of-band performance has a good potential to be utilized in 5G communication systems.

ACKNOWLEDGMENTS

This work was supported by the National Natural Science Foundation of China under Grants 92373202 and 62141409, the National Key Research and Development Program of China under Grant 2019YFB2205003, and the Zhejiang Provincial Key Research & Development Project under Grant 2021C01041.

DATA AVAILABILITY STATEMENT

Data sharing is not applicable to this article as no data sets were generated or analyzed during the current study.

ORCID

Gaofeng Wang http://orcid.org/0000-0001-8599-7249

REFERENCES

1. Jiang Y, Feng L, Zhu H, et al. Bandpass filter with ultra-wide upper stopband on GaAs IPD technology. *IEEE Trans Circuits Syst II Express Briefs*. 2022;69(2):389-393.
2. Liu B-G, Zhou Y-J, Cheng C-H. Miniaturized ultra-wideband bandpass filter with ultra-wide stopband using π-type unit with inductive loading on integrated passive device. *IEEE Trans Circuits Syst II Express Briefs*. 2021;68(11):3406-3410.
3. Chen W, Wu Y, Yang Y, Wang W. IPD-based miniaturized wideband bandpass filter with frequency-dependent complex source and load. *IEEE Trans Plasma Sci*. 2021;49(3):1115-1120.
4. Zhao W, Wu Y, Yang Y, Wang W. LTCC bandpass filter chips with controllable transmission zeros and bandwidths using stepped-impedance stubs. *IEEE Trans Circuits Syst II Express Briefs*. 2022;69(4):2071-2075.
5. Wu Y, Chin K-S, Che W, Chang K-C, Feng W. LTCC multilayered helical filters with a mixed electric and magnetic coupling structure. *IEEE Trans Compon Packag Manuf Technol*. 2015;5(8):1050-1059.
6. Guo Y, Wang H, Fu S, Dou S, Wang W, Wu H. Compact CEBG filter for high-frequency applications with low insertion loss. *IEEE Trans Compon Packag Manuf Technol*. 2023;13(1):99-109.
7. Hou ZJ, Yang Y, Zhu X, Li YC, Dutkiewicz E, Xue Q. A compact and low-loss bandpass filter using self-coupled folded-line resonator with capacitive feeding technique. *IEEE Electron Device Lett*. 2018;39(10):1584-1587.
8. Lyu Y-P, Zhou Y-J, Zhu L, Cheng C-H. Compact and high-order on-chip wideband bandpass filters on multimode resonator in integrated passive device technology. *IEEE Electron Device Lett*. 2022;43(2):196-199.
9. Shen G, Feng W, Che W, Shi Y, Shen Y. Millimeter-wave dual-band bandpass filter with large bandwidth ratio using GaAs-based integrated passive device technology. *IEEE Electron Device Lett*. 2021;42(4):493-496.
10. Wu Y-M, Qiang T, Wang C, Adhikari KK, Lv X, Wu Y. GaAs-based IPD-fabricated center-frequency-controllable bandpass filter with asymmetrical differential inductor and air-bridge enhanced capacitor. *IEEE Access*. 2019;7:137784-137793.
11. Arabi E, Lahti M, Vaha-Heikkila T, Shamim A. A 3-D miniaturized high selectivity bandpass filter in LTCC technology. *IEEE Microw Wirel Compon Lett*. 2014;24(1):8-10.
12. UltraEM V2022, Faraday Dynamics, Inc.; 2022.

How to cite this article: Zhang Q, Cao Y, Wang G. Compact IPD bandpass filter with wide upper stopband based on modified topology for 5G applications. *Microw Opt Technol Lett*. 2024;66:e34259. doi:10.1002/mop.34259